GEOPHYSICS, VOL. 70, NO. 4 (JULY-AUGUST 2005); P. R33–R43, 9 FIGS.
10.1190/1.1993712

Inversion of traveltime data under a statistical model for seismic velocities and layer interfaces

Miguel Bosch[1], Penny Barton[2], Satish C. Singh[3], and Immo Trinks[4]

ABSTRACT

We invert large-aperture seismic reflection and refraction data from a geologically complex area on the northeast Atlantic margin to jointly estimate seismic velocities and depths of major interfaces. Our approach combines this geophysical data information with prior information on seismic compressional velocities and the structural interpretation of seismic sections. We constrain expected seismic velocities in the prior model using information from well logs from a nearby area. The layered structure and prior positions of the interfaces follow information from the seismic section obtained by processing the short offsets. Instead of using a conventional regularization technique to smooth the interface-velocity model, we describe the spatial correlation of interfaces and velocities with a geostatistical model, using a multivariate Gaussian probability density function. We impose a covariance function on the velocity field in each layer and on each interface in the model to control the smoothness of the solution. The inversion is performed by minimizing an objective function with two terms, one term measuring traveltime residuals and the other measuring the fit to the statistical model. We calculate the posterior uncertainties and evaluate the relative influence of data and the prior model on estimated interface depths and seismic velocities. The method results in the estimation of velocity and interface geometry beneath a basaltic sill system down to 7 km depth. This method aims to enhance the interpretation process by combining multidisciplinary information in a quantitative model-based approach.

INTRODUCTION

The estimation of a large-scale velocity model is an important aspect of seismic data analysis and is necessary to generate input for migration or wave-form inversion. However, velocity estimation is not a trivial problem. In seismic reflection analysis, one source of difficulty is the coupling between reflector depths and overlying velocities. Another problem is the spatially irregular ray coverage that results from the acquisition geometry, complex structures, and a heterogeneous velocity field. The velocity estimation can be improved by (1) increasing the offset range, (2) taking into account diving waves in addition to reflections, and (3) providing statistical constraints for the prior mean values and smoothness of model velocities and interfaces.

In recent years several papers have been published (e.g., McCaughey and Singh, 1997; Zelt and Barton, 1998; Hughes et al., 1998; Hobro et al., 2003) that include wide-angle reflection and refraction data in traveltime inversion. In these methods, the model is parameterized using a fine grid, and regularization is applied to constrain the inversion. Tikhonov-type regularization has been the most common approach (Constable et al., 1987; Docherty, 1992; Vasco et al., 1996). It is based on penalizing one particular order of the spatial derivatives of the property, or a linear combination of different orders of the spatial derivatives, by adding a norm of the derivatives to the objective function to be minimized with the inversion, thus raising the problem of which derivative orders or particular linear combination to choose (Zhang and Toksöz, 1998). Another approach to smoothing the model is based on the truncation of singular values of the normal equations. Stork (1992) and Michelena (1993) show that this method is able to adapt the smoothing to the acquisition geometry and irregular gridding, but it is not very efficient for a large number of model parameters.

Manuscript received by the Editor September 23, 2003; revised manuscript received October 10, 2004; published online July 7, 2005.
[1]Formerly Bullard Laboratories, University of Cambridge, Department of Earth Sciences, Madingly Road, Cambridge CB3 0EZ, United Kingdom; presently Universidad Central de Venezuela, Department of Applied Physics, Caracas, Venezuela. E-mail: mbosch@reacciun.ve.
[2]Bullard Laboratories, University of Cambridge, Department of Earth Sciences, Madingly Road, Cambridge CB3 0EZ, United Kingdom. E-mail: barton@esc.cam.ac.uk.
[3]Laboratoire de Geosciences Marines, Institut de Physique du Globe, 4 Place Jussieu, 75252 Paris, Cedex 05, France. singh@ipgp.jussieu.fr.
[4]Formerly Bullard Laboratories, University of Cambridge, Department of Earth Sciences, Madingly Road, Cambridge CB3 0EZ, United Kingdom; presently University of Durham, Department of Earth Sciences, Durham DH1 3LE, United Kingdom. E-mail: immo.trinks@durham.ac.uk.

We propose an alternative approach based on geostatistical methods that characterize the modeled property fields. With up to second-order statistics, such as expected values, variances, and spatial covariances (or equivalently, spatial variograms), significant features of the variability, smoothness, and texture of the property field can be described. Recently, several authors have used geostatistical information in inversion based on Monte Carlo algorithms. The work by Bosch (1999), Bosch and McGaughey (2001), and Bosch et al. (2001) combines geostatistical information, including spatial correlation description, with geophysical data for inversion. Statistical prior information based on outcrop data has been used by Mosegaard et al. (1997) for inversion of seismic data, and several authors have worked on geostatistical inversion of seismic data for estimation of elastic parameters in reservoirs (Hass and Dubrule, 1994; Torres-Verdin et al., 1999; Bosch, 2004).

From a mathematical point of view, there is an equivalence between the description of spatial smoothness of property fields via covariance functions (geostatistical approach) and via the minimization of spatial derivatives (Tikhonov regularization). This equivalency can be extended to other common types of spatial modeling, such as harmonic- or polynomial-based fields [see work by Dubrule (2003) and Chiles and Delfiner (1999) for more information on this subject]. The geostatistical description, however, fits naturally within the framework of statistical inversion. Additionally, from a practical point of view, it seems simpler to understand the relationship between property field appearance and spatial covariances (Isaaks and Srivastava, 1989; Deutsch and Journel, 1992) than its relationship with conditions on spatial derivatives.

The spatial resolution achieved in traveltime tomography is very heterogeneous, depending on several factors, such as raypath coverage, diversity in ray directions, and Fresnel zone radius. Given the practical importance of accounting for this heterogeneity in the inversion, some authors have followed variable, adaptive, or multiscale parameterization approaches for spatial resolution problems (Böhm and Vesnaver, 1999; Böhm et al., 2000; Zhou, 2003; Trinks et al., 2004). In order to introduce a variable regularization, our method allows a choice of type and range of the covariance function used in the statistical model for each layer and interface. One advantage of this approach is that we do not need to adapt the parameterization by introducing variable cell sizes or variable node separations.

In this paper, we describe the application of a geostatistical model to layer velocities and interfaces for nonlinear inversion of seismic traveltime data. The information required for the definition of prior mean values and deviations of velocity parameters is based on well data. The layered model and prior mean values for interface depths are derived from processed seismic data. Other parameters of the statistical model, such as the covariance functions, are fixed to values that produce a model consistent with the resolution of the traveltime tomography. We use Newton's method to find an optimal model that jointly honors the statistical model and explains the traveltime data. We apply this approach to a seismic profile from the northeast Atlantic margin, including traveltimes for reflections and diving waves that have been identified up to offsets of 20 km.

GEOSTATISTICAL INVERSION

Our method is based on Bayesian inversion of traveltimes, which allows the user to combine data and prior information. The general formulation is given in terms of the posterior probability density:

$$\sigma(\mathbf{m}) = c\,\rho(\mathbf{m})\,L(\mathbf{m}), \tag{1}$$

where $\mathbf{m}$ is the model parameter array, $\sigma(\mathbf{m})$ is the posterior probability density, $\rho(\mathbf{m})$ is the prior probability density, $L(\mathbf{m})$ is the likelihood function, and c is a normalization constant (Tarantola, 1987). The prior probability density represents the information on the media model before fitting the traveltime data. The posterior probability density includes the prior information and the information provided by the traveltime observations. We model the prior information density with a multivariate Gaussian function with mean $\mathbf{m}_{\text{prior}}$ and model covariance matrix $\mathbf{C}_{\text{m}}$:

$$\rho(\mathbf{m}) = c \exp\left[-\frac{(\mathbf{m}-\mathbf{m}_{\text{prior}})^{\text{T}}\mathbf{C}_{\text{m}}^{-1}(\mathbf{m}-\mathbf{m}_{\text{prior}})}{2}\right], \tag{2}$$

which is commonly used in geostatistics to describe spatially distributed property fields. The information on the variability and the spatial correlation of the model parameters is contained in the covariance matrix. The diagonal elements in $\mathbf{C}_{\text{m}}$ are the variances and describe the variability of the parameters from the mean values. The nondiagonal terms in $\mathbf{C}_{\text{m}}$ describe the spatial correlation of the velocity field and are calculated from a covariance function model. In most geophysical work using a multivariate Gaussian prior model, the parameters are considered spatially independent, and hence the prior model covariance matrix is usually a diagonal matrix. In our approach, the velocities and the interface depths are spatially correlated; therefore, $\mathbf{C}_{\text{m}}$ is nondiagonal.

The likelihood function is described here as a Gaussian function

$$L(\mathbf{m}) = \exp\left\{-\frac{[\mathbf{d}_{\text{obs}}-\mathbf{g}(\mathbf{m})]^{\text{T}}\mathbf{C}_{\text{d}}^{-1}[\mathbf{d}_{\text{obs}}-\mathbf{g}(\mathbf{m})]}{2}\right\}, \tag{3}$$

where $\mathbf{d}_{\text{obs}}$ are the observed data, and $\mathbf{g}(\mathbf{m})$ are the traveltime data calculated from the model by solving the forward problem. We consider data uncertainties to be independent; therefore, the covariance data matrix $\mathbf{C}_{\text{d}}$ is diagonal. The independent nature of data errors has been a common assumption in seismic tomography. However, this independence is not an intrinsic limitation of the method presented here, since we carry the full data covariance matrix in all formulae below.

We are considering here the prior centroid and the covariances as known parameters of the statistical model. In a more complex formulation, they may be considered hyperparameters, also subject to probability distributions. An example of this approach is the work on wavelet estimation by Buland and Omre (2003) using Monte Carlo methods.

Our inverse problem is based on the determination of model parameters that maximize the posterior probability. This process is equivalent to the minimization of the

following objective function:

$$S = \underbrace{\frac{[\mathbf{g}(\mathbf{m}) - \mathbf{d}_{\text{obs}}]^{\text{T}}\mathbf{C}_{\text{d}}^{-1}[\mathbf{g}(\mathbf{m}) - \mathbf{d}_{\text{obs}}]}{2}}_{\text{geophysical objective}} + \underbrace{\frac{(\mathbf{m} - \mathbf{m}_{\text{prior}})^{\text{T}}\mathbf{C}_{\text{m}}^{-1}(\mathbf{m} - \mathbf{m}_{\text{prior}})}{2}}_{\text{geostatistical objective}}, \quad (4)$$

The first term of the objective function describes the fit of the observed data with calculated data for a particular model **m**. The second term describes how well the model complies with the geostatistical information. The relative influence of each term in the objective function is controlled by the data and model variances, respectively, and is given in the diagonal elements of the covariance matrix. The smaller the variance, the larger the influence of the corresponding term in the objective function will be.

To minimize the objective function, we use an iterative approach that involves linearizing the traveltime function **g**(**m**), calculating a model perturbation, and repeating the procedure until convergence is obtained. The expression for the gradient of the objective function is obtained by differentiating the objective function with respect to the model parameters:

$$\nabla S = \mathbf{G}^{\text{T}}\mathbf{C}_{\text{d}}^{-1}[\mathbf{g}(\mathbf{m}) - \mathbf{d}_{\text{obs}}] + \mathbf{C}_{\text{m}}^{-1}(\mathbf{m} - \mathbf{m}_{\text{prior}}), \quad (5)$$

where **G** is the matrix of partial derivatives of the calculated traveltimes with respect to the model parameters. An approximate expression for the Hessian matrix is obtained by differentiating the gradient with respect to the model parameters and neglecting second-order derivatives in **g**(**m**):

$$\mathbf{H}(S) = \mathbf{G}^{\text{T}}\mathbf{C}_{\text{d}}^{-1}\mathbf{G} + \mathbf{C}_{\text{m}}^{-1}. \quad (6)$$

Using Newton's method (Tarantola, 1987), the linear equation $\mathbf{H}(S)\Delta\mathbf{m} = -\nabla S$ can be used to solve for the model perturbation $\Delta\mathbf{m}$:

$$\left(\mathbf{G}^{\text{T}}\mathbf{C}_{\text{d}}^{-1}\mathbf{G} + \mathbf{C}_{\text{m}}^{-1}\right)\Delta\mathbf{m} = \mathbf{C}_{\text{m}}^{-1}(\mathbf{m}_{\text{prior}} - \mathbf{m}) - \mathbf{G}^{\text{T}}\mathbf{C}_{\text{d}}^{-1}[\mathbf{g}(\mathbf{m}) - \mathbf{d}_{\text{obs}}], \quad (7)$$

which can be rewritten as

$$\underbrace{\left(\mathbf{C}_{\text{m}}\mathbf{G}^{\text{T}}\mathbf{C}_{\text{d}}^{-1}\mathbf{G} + \mathbf{I}\right)}_{\text{curvature of } S}\Delta\mathbf{m} = \underbrace{\mathbf{m}_{\text{prior}} - \mathbf{m} - \mathbf{C}_{\text{m}}\mathbf{G}^{\text{T}}\mathbf{C}_{\text{d}}^{-1}[\mathbf{g}(\mathbf{m}) - \mathbf{d}_{\text{obs}}]}_{\text{direction of steepest descent}}, \quad (8)$$

Equation 8 requires the model covariance matrix instead of its inverse. It has, as well, a dimensionless matrix (the curvature of S) on the left-hand side. A biconjugate gradient algorithm (Press et al., 1997) is used to calculate $\Delta\mathbf{m}$ by solving the linear system of equations that is given by expression 8. Any algorithm used to solve this system of equations needs to comply with nonsymmetric matrices since the curvature of S is a nonsymmetric matrix; therefore, a plain conjugate-gradient algorithm would not be adequate.

POSTERIOR UNCERTAINTIES AND RESOLUTION

It is useful to derive error bars for the solution obtained with nonlinear optimization procedures, such as the one described here, and to analyze the influence of prior information and data. In principle, a full description of posterior uncertainties and the shape of the posterior density could be achieved using Monte Carlo exploration methods, which are not treated here. We study uncertainty and resolution on the linear approximation of the traveltime forward problem around the optimal model. All posterior statistics mentioned below refer to this approach.

With the forward problem being linear, the likelihood function, equation 3, is Gaussian. Thus, the posterior density, equation 1, is also Gaussian. In this approximation, the posterior covariance matrix is the inverse of the Hessian matrix, and its diagonal elements are the posterior variances of the model parameters. The calculation of posterior uncertainties by inverting the Hessian matrix requires the inversion of two matrices: the prior covariance matrix term of the Hessian and the Hessian itself. A more efficient way to perform the calculation is to use the curvature matrix $\mathbf{A} = (\mathbf{C}_{\text{m}}\mathbf{G}^{\text{T}}\mathbf{C}_{\text{d}}^{-1}\mathbf{G} + \mathbf{I})$. The inverse of the Hessian can then be obtained from, $\mathbf{H}(S)^{-1} = \mathbf{A}^{-1}\mathbf{C}_{\text{m}}$, requiring the inverse of only one matrix.

As our technique combines geostatistical and geophysical information, it is important to address the issue of the relative influence of each one in the estimation of velocities and interface depths. The importance of prior information in geophysical inference has been a matter of discussion (e.g., Scales and Sneider, 1997; Scales and Tenorio, 2001). The relative influence is spatially variable since the resolution provided by the geophysical data depends on the ray coverage: the estimated property field in nonilluminated areas of the model (i.e., far from raypaths) should be influenced only by the geostatistical information, whereas in densely illuminated areas, it is largely influenced by the geophysical data.

To evaluate this problem, we consider a true model, $\mathbf{m}_{\text{true}}$, such that the observed data is $\mathbf{d}_{\text{obs}} = \mathbf{g}(\mathbf{m}_{\text{true}})$, a perturbed true model, $\mathbf{m}_{\text{true}} + \delta\mathbf{m}_{\text{true}}$, with observed data, $\mathbf{d}_{\text{obs}} + \delta\mathbf{d}_{\text{obs}} \approx \mathbf{d}_{\text{obs}} + \mathbf{G}\delta\mathbf{m}_{\text{true}}$, and a perturbed prior model is $\mathbf{m}_{\text{prior}} + \delta\mathbf{m}_{\text{prior}}$. We assume that prior and true model perturbations follow the geostatistics defined by the model prior information. The corresponding expression for the model update, equation 8, after these perturbations is

$$\left(\mathbf{C}_{\text{m}}\mathbf{G}^{\text{T}}\mathbf{C}_{\text{d}}^{-1}\mathbf{G} + \mathbf{I}\right)(\Delta\mathbf{m} + \delta\mathbf{m}) = \mathbf{m}_{\text{prior}} + \delta\mathbf{m}_{\text{prior}} - \mathbf{m} - \mathbf{C}_{\text{m}}\mathbf{G}^{\text{T}}\mathbf{C}_{\text{d}}^{-1}[\mathbf{g}(\mathbf{m}) - \mathbf{d}_{\text{obs}} - \mathbf{G}\delta\mathbf{m}_{\text{true}}), \quad (9)$$

with $\delta\mathbf{m}$ being the difference between the estimated model updates for the perturbed and unperturbed prior and true models. By subtracting equation 8 from equation 9, we obtain the expression for the estimated model perturbation:

$$\left(\mathbf{C}_{\text{m}}\mathbf{G}^{\text{T}}\mathbf{C}_{\text{d}}^{-1}\mathbf{G} + \mathbf{I}\right)\delta\mathbf{m} = \delta\mathbf{m}_{\text{prior}} + \mathbf{C}_{\text{m}}\mathbf{G}^{\text{T}}\mathbf{C}_{\text{d}}^{-1}\mathbf{G}\delta\mathbf{m}_{\text{true}}. \quad (10)$$

Again, using the notation **A** for the curvature matrix at the left-hand side, multiplying by the inverse of **A**, and recognizing the matrix (**A** – **I**) in the right-hand side of the geophysical data term, we obtain the expression

$$\delta\mathbf{m} = \mathbf{A}^{-1}\delta\mathbf{m}_{\text{prior}} + (\mathbf{I} - \mathbf{A}^{-1})\delta\mathbf{m}_{\text{true}}. \quad (11)$$

Equation 11 describes how a perturbation of the expected prior model and a perturbation of the true model expressed through the geophysical data are combined to give a perturbation of the solution within the validity of the linear approximation of the forward problem.

We are interested in analyzing the effect on the estimated model of both prior and true model perturbations that comply with the spatial correlation defined for each layer and interface, i.e., multivariate Gaussian with covariance matrix $\mathbf{C}_m$. Gaussian spatially correlated perturbations are obtained by the common method of the square root of the correlation matrix (e.g., Davis, 1987; Dietrich, 1993) $\delta\mathbf{m}_{prior} = \mathbf{R}_m^{1/2}\delta\tilde{\mathbf{m}}_{prior}$ and $\delta\mathbf{m}_{true} = \mathbf{R}_m^{1/2}\delta\tilde{\mathbf{m}}_{true}$, where $\mathbf{R}_m$ is the model correlation matrix and $\delta\tilde{\mathbf{m}}_{prior}$ and $\delta\tilde{\mathbf{m}}_{true}$ are multivariate independent (i.e., spatially uncorrelated) Gaussian deviates of zero mean and variance given by the diagonal elements of the model covariance matrix, $\mathbf{C}_m$. Making the corresponding substitution in equation 11 we obtain

$$\delta\mathbf{m} = \underbrace{\mathbf{A}^{-1}\mathbf{R}_m^{1/2}}_{\substack{\text{prior}\\ \text{information}\\ \text{contribution}}}\delta\tilde{\mathbf{m}}_{prior} + \underbrace{(\mathbf{I}-\mathbf{A}^{-1})\mathbf{R}_m^{1/2}}_{\substack{\text{geophysical}\\ \text{information}\\ \text{contribution}}}\delta\tilde{\mathbf{m}}_{true}, \qquad (12)$$

Equation 12 shows that decorrelated prior and true model perturbations linearly combine to give the inversion solution, with the corresponding weighting matrices $\mathbf{A}^{-1}\mathbf{R}_m^{1/2}$ and $(\mathbf{I}-\mathbf{A}^{-1})\mathbf{R}_m^{1/2}$. These two matrices describe the relative influence of prior and geophysical information, respectively. Note that the two matrices sum to the square root of the correlation matrix, which means that the contributions are complementary. In particular, as the square-root correlation matrix has the value of one in the diagonal, corresponding elements of the diagonals of the two matrices (geophysical information and prior information) add to a total of one.

To easily understand the meaning of the matrix coefficients in linear equation 12, it is useful to consider the specific cases of prior and true model perturbations centered at arbitrary parameters i and j, correspondingly, and having the typical size defined by the correlation function. These perturbations correspond to $\delta\mathbf{m}_i = \mathbf{R}_m^{1/2}\delta_i$, and $\delta\mathbf{m}_j = \mathbf{R}_m^{1/2}\delta_j$, with δ_i being of value one for the ith parameter and zero for the other parameters, and δ_j being the equivalent for the jth parameter. Thus, in this case we have the model solution perturbed by

$$\delta\mathbf{m}_{ij} = \underbrace{\mathbf{A}^{-1}\mathbf{R}_m^{1/2}}_{\substack{\text{prior}\\ \text{information}\\ \text{contribution}}}\delta_i + \underbrace{(\mathbf{I}-\mathbf{A}^{-1})\mathbf{R}_m^{1/2}}_{\substack{\text{geophysical}\\ \text{information}\\ \text{contribution}}}\delta_j, \qquad (13)$$

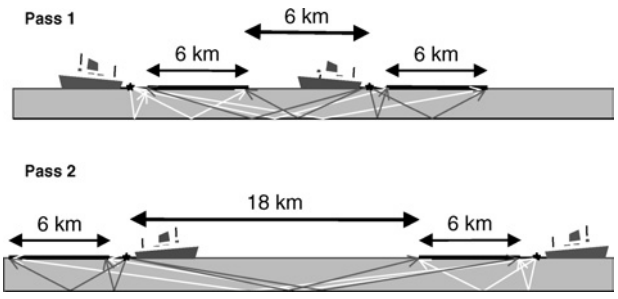

Figure 1. Acquisition geometry used in the seismic experiment to obtain a large range of offsets from 200 m to 30 km. Pass 1: 0–6 km, 6–12 km, and 12–18 km. Pass 2: 0–6 km, 18–24 km, and 24–30 km.

where *i*th column of the first matrix, $\mathbf{A}^{-1}\mathbf{R}_m^{1/2}$, is the perturbation caused by the prior model, and the *j*th column of the second matrix, $(\mathbf{I}-\mathbf{A}^{-1})\mathbf{R}_m^{1/2}$, is the perturbation caused by the geophysical data.

Notice that expression 13 evaluates the influence on estimated model parameters caused by single prior or true model features of regular size according to the model spatial correlation, and expression 12 evaluates the influence caused by arbitrary prior or true model features that honor the spatial correlations given in the geostatistical model. In contrast, expression 11 evaluates the influence on estimated parameters caused by independent parameter variations in the true or prior model. For the particular case of spatial statistical independence across model parameters (i.e., diagonal model covariance matrix), the correlation matrix $\mathbf{R}_m$ is the identity matrix; hence, the geophysical information contribution (the last term in expressions 12 and 13) is simply $\mathbf{I}-\mathbf{A}^{-1}$, which is the common data resolution matrix (Backus and Gilbert, 1968) used in standard geophysical inversion. It is a particular case of our formulation that accounts for spatially related model parameters.

SEISMIC DATA

We use data collected during a wide-aperture seismic experiment along a seismic profile over the northeast Atlantic margin. These data were acquired using a two-ship, two-pass geometry with both vessels towing 6-m-long streamers and sources. The separation between the vessels during the first pass was 6 km, providing an offset range of 18 km. For the second pass, the separation was increased to 18 km, leading to a total offset coverage from 200 m to 30 km (see Figure 1).

Figure 2a shows the near-offset (6-km) stacked section, after poststack depth migration, with the major structural features in the area indicated. Three continuous sedimentary layers can be seen above a series of high-amplitude discontinuous reflectors. Deep reflectors are obscured by seabed multiples. Strong reflectors between 3.5 km and 5 km depth correspond to a system of sills — discontinuous layers of laminar basalt intrusions ranging from several tens of meters to 100 m thick, which typically intrude surfaces of weakness within the sedimentary layers, such as faults or sedimentation surfaces. Sills may sometimes form horizontally branched Christmas-tree-type structures with several levels. Continuous events below the sills are multiples of reflectors above.

The velocity model used for stacking and migration (Figure 2b) was obtained by conventional normal-moveout (NMO) semblance analysis of common-depth-point (CDP) gathers. This velocity field is poorly constrained beneath the basaltic sills and inaccurate for the layer just above the sills because of the complex geometry of sill reflectors, although it is much better constrained for the three shallower continuous layers. In this work, we are using traveltime tomography to produce an alternative velocity model.

Since the model under consideration consists of sedimentary layers, sills, and a basement, we parameterized the model with corresponding layers separated by interfaces. The geostatistical description of the velocity (expected values, variances, and spatial covariances) is independent for each layer and for each interface. The velocities and interfaces were modeled using cubic splines (Hobro et al., 2003), and the traveltimes

were calculated with a ray-tracing methodology (Farra , 1990; Hobro et al., 2003).

Although reflections from the sills are discontinuous, we included traveltimes of some of these reflectors in the inversion since they provide useful constraints on the velocity of the upper layers. To include these reflectors in the model, we used a continuous interface, representing only one level of sill and connecting neighboring sills. We refer to this interface as a pseudo-interface to differentiate it from the lithologically continuous interfaces bounding layers 1 to 3. For diving rays transmitted below this pseudo-interface, we impose velocity continuity across it, which is the same as considering the absence of sills for deeper phases. This is justified because the sills are not present everywhere, and their typical thickness is from 80 to 100 m, producing a relatively small one-way traveltime effect on traversing rays (approximately 8 ms) that has been included in the data uncertainties for the diving-ray phases (75 ms). Thus, the pseudo-interface represented in the model has only the effect of providing a reflection surface for the simulation of the selected sill events; its influence on other phases is negligible.

The model array, **m** in equations 1–13, includes a description of the velocities for each layer and each interface. Parameters corresponding to the same velocity layer or the same interface are considered spatially dependent and statistically homogeneous, whereas parameters of different layers or interfaces are considered statistically independent, with the exception of velocities in layers 4 and 5. In the latter case, velocities are considered spatially correlated across these two layers to model sills embedded in a continuous sedimentary medium, as discussed previously. In this application, we are dealing with approximately 5000 model parameters, including layer velocity and interface depth parameters.

Figure 3 shows a typical shot supergather and some data picked for the inversion. Traveltime data were picked manually for sources at 1-km intervals. We used manual picking because of the discontinuity of the sills and deeper reflectors and the low S/N for long-offset arrivals. Short-offset-reflected phases 1, 2, and 3 correspond to the bases of layers 1, 2, and 3 shown on the stacked section (Figure 2a), and phase 4 corresponds to the strong reflection from the sills. At longer offset, phases 5, 6, and 7 correspond to diving rays turning progressively at greater depths. No strong arrivals were observed beyond 20-km offset. Zero-offset traveltimes picked from the stacked section for all interfaces except the basement interface are also used in the inversion.

Data variances (i.e., the diagonal entries of matrix $\mathbf{C}_d$ in equation 9) result from the accumulation of errors from time recording, phase identification, time picking, and calculation. Because of the relatively small traveltime sampling interval (4 ms) and calculation error (less than 4 ms), the dominant components of our data errors correspond to the phase identification and time pick. To account for these uncertainties, we use a data standard deviation of half a dominant period (25 ms) for reflections and a dominant period (75 ms) for diving waves.

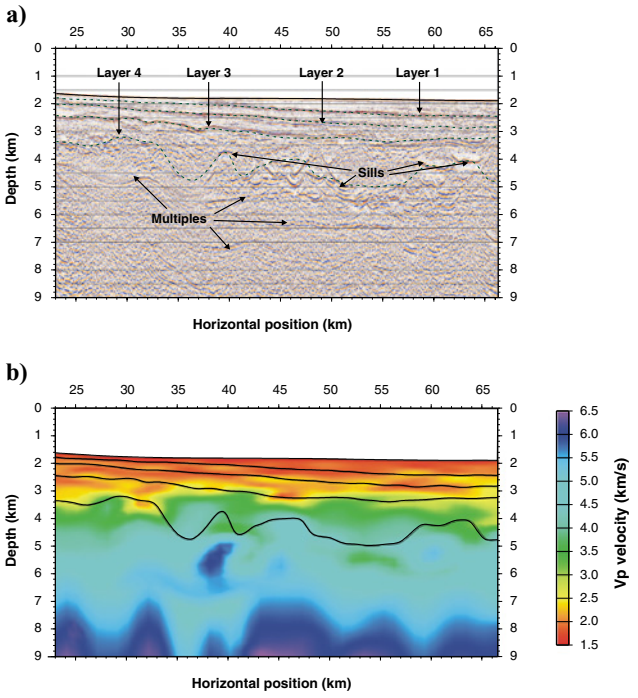

Figure 2. (a) Poststack depth-migrated seismic section in the area showing major structures used to define the layered model for the traveltime inversion. Layers are separated by continuous interfaces (dotted dark green). (b) Interval velocities derived from the stacking-velocity model and used for the migration shown in (a). Lines show (prior) layered model interpreted from the seismic section, shown dotted dark green in (a).

GEOSTATISTICAL INFORMATION

The geostatistical information provided for each layer in the model consists of (1) an estimation of the velocities and interface depths, (2) their uncertainties, and (3) a description of the spatial correlation of the modeled properties with the covariance function and ranges. Concerning the covariance functions, we used a Gaussian covariance function for all velocity layers and interfaces with the exception of the pseudo-interface marking sill reflectors, where we used an exponential covariance function appropriate for the rough character and

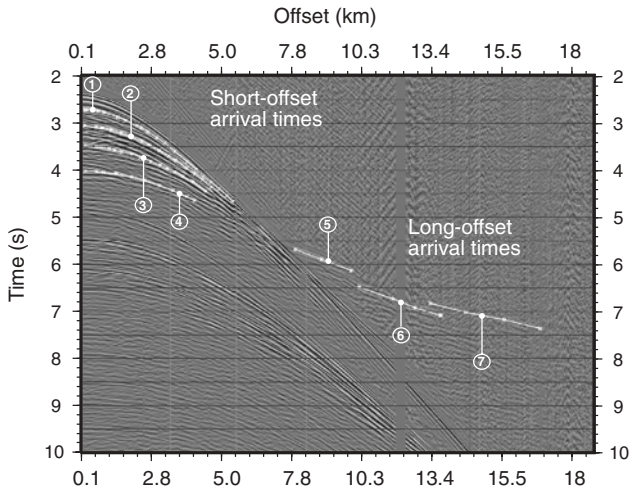

Figure 3. Shot supergather showing four selected events at short offset and three at long offset used for the traveltime inversion.

discontinuity of the sills. The choice of covariance functions and their ranges is part of our geostatistical model assumptions.

Although there are no wells along this line, we had access to confidential well information from a nearby area. We had access only to crossplots of the P-wave velocity with depth below the seafloor, containing sand, shale, limestone, and basalt data. Combining this information with interval velocities derived from stacking velocities, we were able to tentatively associate the three shallower layers with clastics and the two consecutive sedimentary layers (layer 4 above the sills and 5 below the sills) with clastics and limestone. From the crossplots, we extracted the linear trend of the velocity with depth below seafloor for clastics and clastics with limestone. We used these trends for the prior expected velocities and their variance in the three shallower layers and layers 4 and 5, respectively. Prior uncertainties (one standard deviation) for velocities were 0.2 km/s for the three shallower sedimentary layers, 0.3 km/s for the two consecutive layers (sediments above and below the sill system), and 0.1 km/s for the basement.

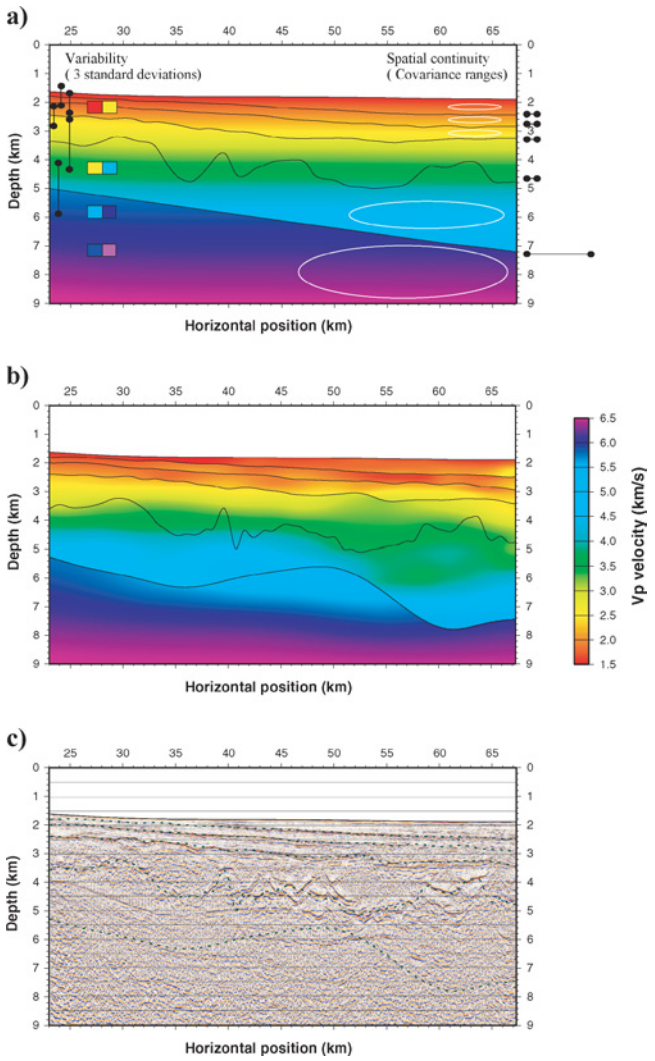

Figure 4. (a) Description of the statistical model input as prior information for the inversion. The expected velocities are plotted with colors and the expected depths of the interfaces with continuous lines. The variabilities of interface depths are shown with vertical lines ending with black circles; the line size corresponds to ±3 standard deviations. The variabilities of the compressional velocities are indicated at three positions by two-color boxes showing ±3 standard deviations. The ellipses show ranges of spatial continuity (covariance function ranges) for the velocity field. The covariance ranges for the interface depths are shown with horizontal lines ending with black circles to the right side of the figure. (b) Model obtained after the geostatistical inversion of traveltimes. (c) Seismic section poststack depth migrated with the velocity field shown in (b). Interface depths estimated from the inversion are superimposed (dotted dark green).

The velocity model obtained from stacking velocities was not used for definition of the prior values of the velocity field or the variances. We preferred information from the crossplots of well log data, which was independent from the seismic data. Additionally, the crossplots presented well log data down to 5 km depth below the seabed, whereas the stacking velocities were poorly constrained below 2.5 km depth below the seabed.

The prior model for interface depths was constructed from interface positions from the processed seismic section. These depths are affected by uncertainties in the velocity model obtained from stacking velocities and used for migration. We assigned uncertainties to the prior interface depths to accommodate these errors. Prior uncertainties (one standard deviation) for interface depths were 50 m for the seabed, 100 m for the three shallower reflectors, and 300 m for the sill pseudo-interface and the basement. An interface for the basement was not visible on the processed seismic section. After tests performed with ray tracing, we found that a basement dipping toward the east was needed to explain the phase with longest offset arrivals.

Figure 4a shows a compilation of information defining the geostatistical model given as input to the inversion. The plotted velocity field corresponds to the expected values for the velocities and interfaces, which were obtained from the velocity-versus-depth plots for different types of sediments. Also, deviations from the velocity (shown as colored boxes in each layer) were obtained from these crossplots. The ellipses in the figure describe the range of spatial covariance of the velocity field, showing the size of the covariance ranges in the vertical and horizontal directions for each layer. The smoothness of each interface is controlled by the covariance function model and range, shown by bars to the right side of the figure. With our choice of ranges, we demanded smoother velocities and interface geometry for the bottom part of the model and allowed higher spatial resolution for the shallower part of the model.

For traveltime inversion, it is necessary to consider the minimum size of features that can be resolved by the inversion, which depends on data quality and ray density. Diversity in ray directions (crossing of rays) is also important to contribute independent linear equations to the Frechet derivative matrix. We adapt model smoothness to the decreasing spatial resolution of the tomography with depth by the definition of the covariance function, allowing us to account for the reduction of ray coverage with depth (see Figure 5) and the enlargement of the Fresnel zone for deeper rays (Hubral et al., 1993; Spetzler and Snieder, 2004). The Fresnel zone in our experiment has a

diameter of as much as 0.7 km for rays in the shallower layers and as much as 1.5 km for the deepest rays.

For the first three sedimentary layers, we use spatial covariance ranges of 3 km for the horizontal direction and 200 m for the vertical direction, which is consistent with structure and stratigraphy in these layers, where vertical variations have a much shorter range than horizontal variations. For layer 4 (above the sills) and layer 5 (below the sills), covariance ranges for the velocity were larger: 15 km in the horizontal and 1 km in the vertical direction. For the basement (layer 6), longer covariance ranges were used to estimate a very smooth velocity field — a horizontal range of 20 km and a vertical range of 2 km. The pseudo-interface marking sill reflectors was characterized using a 3-km covariance range, which is coherent with the size of sill reflectors in the stacked section and the fact that this interface is well illuminated by reflecting rays. The basement interface is modeled with a range of 12 km to estimate a very smooth surface because only the last data phase reaches this interface, and ray density is much lower than for other interfaces.

For convenience, we sometimes present uncertainties in different standard-deviation criteria. In Figure 4a, we present three standard deviations (3-sigma criterion); in figures discussed later, we use one standard deviation (1-sigma criterion). Standard deviations mark probabilities (confidence intervals) of 0.682, 0.954, and 0.997 for the 1, 2, and 3-sigma criteria, correspondingly. Hence, the 1-sigma criterion should be regarded as a soft boundary, and the 3-sigma criterion as a hard boundary.

TOMOGRAPHY RESULTS

Inversion proceeds by simultaneous adjustment of the velocity field and the depth of the interfaces between layers to improve the data fit, using the prior model as the initial model. The following three steps were used to simplify the inversion: first, the velocities and interface depths for the three upper layers were jointly inverted using the traveltime data of the three earlier phases; second, with these shallower layers fixed, we inverted the traveltime data of the remaining four phases to jointly estimate the velocities for layers 4, 5, and 6, the depths for the sill, and the basement interface; third, we iterated the inversion for additional adjustment of our most complex interface, the sill pseudo-interface, keeping the other parameters fixed. The overall data fit improved about eight times during the inversion, from 9.3 average datum chi-squared misfit for the initial model to 1.2 for the final model, all data phases included.

Figure 4b shows the final model. Compared with the prior model (Figure 4a), the final model shows significant spatial heterogeneities in the velocity and more detailed structures in the shapes of all the interfaces. For the three upper sedimentary layers, the velocities are slower than prior velocities, and the interfaces are shallower. The fourth interface is more clearly defined, and the basement proves to have a marked structure that we interpret as a large basement block. Compared with the velocity model derived from conventional velocity analysis (Figure 2b), the final model is smoother. Heterogeneities in the three shallower layers are particularly similar across these two models (Figures 2b and 4b); for example, the velocity inversion at the top of the second sedimentary layer between the coordinates of 50 and 60 km. However, there is significant difference for layers below the third interface, where velocities obtained through velocity analysis are less reliable because of the complex geometry of the sill reflectors and the poor constraints below the sills. Tomographic results show slower velocities in layers above and below the sills than corresponding velocities obtained through semblance velocity analysis.

Ray tracing demonstrates that the data provide significant ray coverage down to 7–8 km depth. Figure 5 shows rays traced for the different data phases used in the inversion and how these phases transmit through the model at different depths. The structure beneath approximately 5 km depth is constrained by long-offset arrivals alone, highlighting the relevance of the long-offset seismic information in construction of the deeper part of the model. In particular, the longest offset refracted arrival shows significant variation in arrival time along the profile, allowing an estimation of the deep basement structure.

The seismic velocities in the optimal model obtained with the inversion honor the information on spatial continuity as well as the statistics of the mean values. Figure 6 shows crossplots of the estimated velocities versus depths below the sea bottom corresponding to the posterior model (Figure 4b). The central line in the figure indicates the expected values of the velocity given in the geostatistical model; velocities in the geostatistical prior model (Figure 4a) correspond to this central line. It is important to note that the inversion adjusted the calculated traveltimes while keeping velocities well within the statistics provided as prior information.

We evaluate the confidence on the estimated velocity model by calculating the uncertainties (Figure 7a). The posterior uncertainties are naturally heterogeneous within the section because of variations in ray coverage. Certainty increases toward the center of the section. To the sides of the section, the posterior velocity uncertainties tend toward the prior velocity uncertainties, as expected.

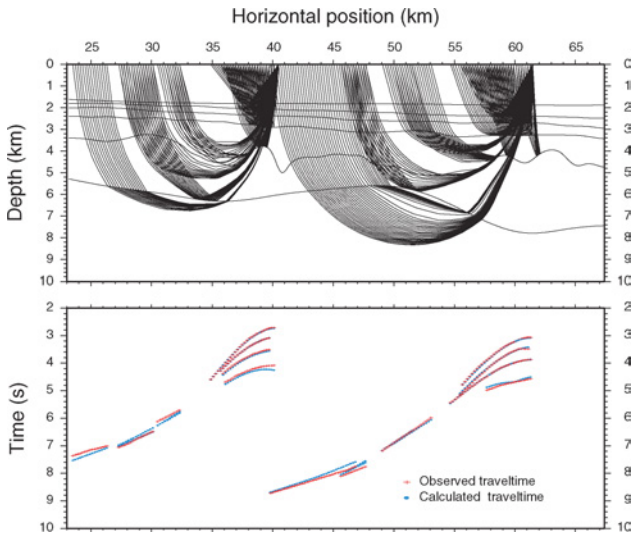

Figure 5. Rays and traveltimes in the inverted velocity-structural model for two example-shot super-gathers (shots at 40.5 km and 61.5 km).

As this methodology combines geostatistical prior information and geophysical information, it is important to identify the relative influence of each type of information on the different features of the estimated model. Figure 7b shows the relative influence of geophysical information and the prior model on the estimated velocities of the model presented in Figure 4b. The influence of the geophysical information is shown to be larger in areas of better ray coverage and negligible at the sides of the section, as expected. As explained before, data and prior information influences add to unity; hence, wherever the influence of data in the estimation is small, the influence of the prior information is large, and vice versa, so that the two influences complement each other.

Figure 8a shows posterior and prior uncertainty bands (one standard deviation) for interface depths, illustrating the modification of the expected value (center of the bands) and the reduction of the posterior uncertainty caused by the new information incorporated by the geophysical data. Figure 8b shows the relative influence of geophysical information and prior information on the estimation of interface depths. The plots indicate that the interfaces are generally well constrained by the traveltime data, except at the sides of the section. Shallower interfaces are better constrained by data than deeper interfaces. This is a reasonable result because (1) deeper interfaces are illuminated by fewer rays, and (2) the longer the ray, the greater the influence of the velocity field on the traveltime and the more important the velocity-interface depth trade-off.

A comparison between the influences of geophysical data and posterior uncertainties on interfaces and velocities shows

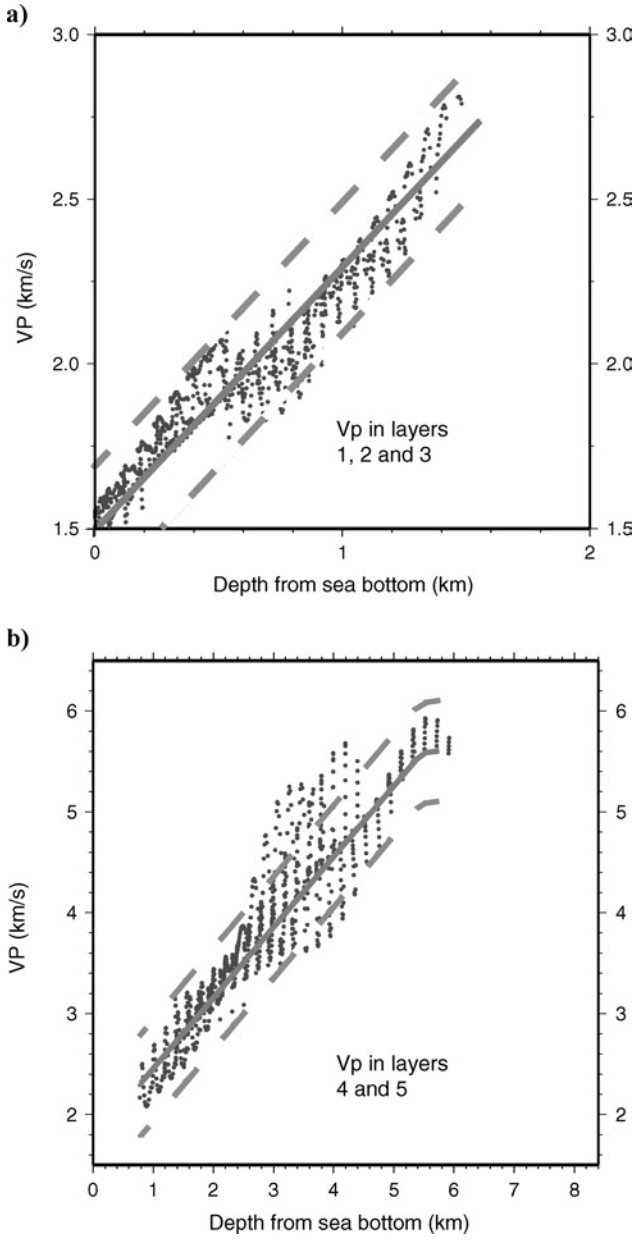

Figure 6. Crossplots of the estimated seismic velocities (dots) versus depth from the seafloor in (a) layers 1, 2, and 3, and (b) layers 4 and 5, showing deviations from the central values provided as prior information (solid line). Dotted lines show one standard deviation from the central values used to constrain the velocities in the prior statistics.

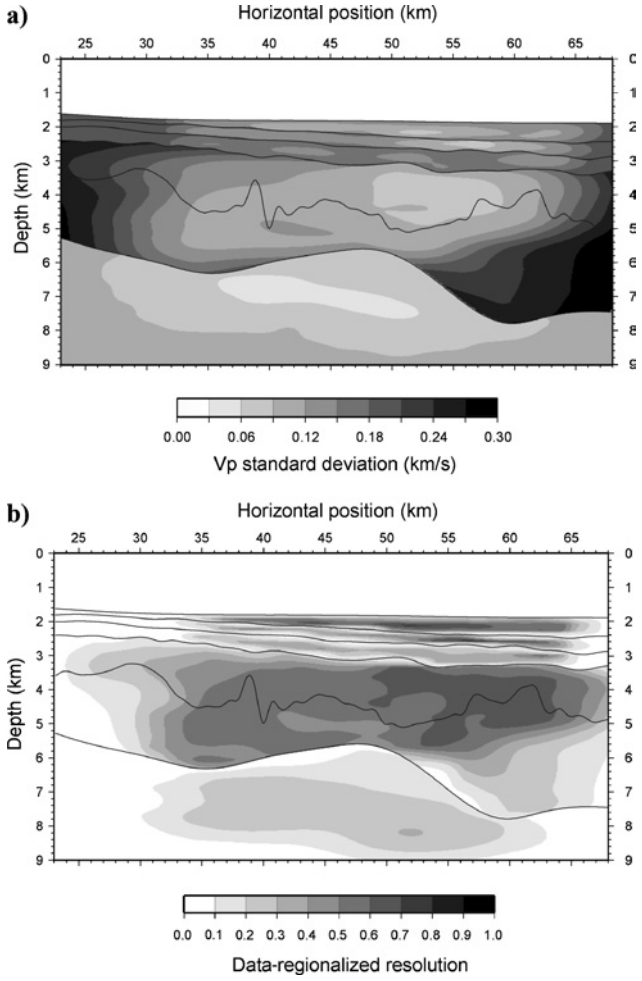

Figure 7. (a) Plot of the posterior uncertainties (one standard deviation) associated with the estimated velocities. Values to the side of the section equal the prior velocity uncertainty of 0.2 km/s for the first three layers, 0.3 km/s for the layers above and below the sills, and 0.1 km/s for the basement velocities. (b) Plot of the impact of traveltime data on the estimated velocities. Impact of the prior information is the complement to unity at each location.

that the impact of data is generally greater on the depths of interfaces than on velocities; this is because, within the framework defined by the prior standard deviation for velocities and depths, the effect on traveltimes is larger for an interface-depth variation than for an equally probable velocity variation. The same conclusion has been reached in previous work (e.g., Rossi et al., 2001) on seismic tomography resolution.

The final velocity field complies with the traveltime information — short and long offsets — and the geostatistical information. We use the velocities estimated with the tomography (Figure 4b) to poststack depth migrate the seismic data (Figure 4c, overlaid with the estimated interface positions). In the shallow part, both the migrated section and the tomographic model delineate the three major upper sedimentary layers and the system of sills. Figure 4c shows the sill reflections between 3 and 6 km depth, and it is interesting to note the coincidence of the migrated and tomographic positions for many of the sills. We highlighted before that the pseudo-interface represented in the model marked some sill reflections that are correctly positioned here. Other sill reflectors are positioned shallower or deeper, in some cases forming a horizontally branched Christmas-tree-type structure; these sills were not represented in the model or in the data used in the inversion.

The effect of the improved velocities on the seismic image is significant, particularly for events beneath the three upper-most layers. Comparing Figures 2a and 4c, we see corrections in the positions of sill reflectors over several hundred meters, and the image underneath the sills also has improved. A detail is shown in Figure 9, where complex reflectors beneath the sills were clearly over-migrated with the stacking velocity model (Figure 9a) and better imaged with the velocity model obtained through tomographic inversion (Figure 9b).

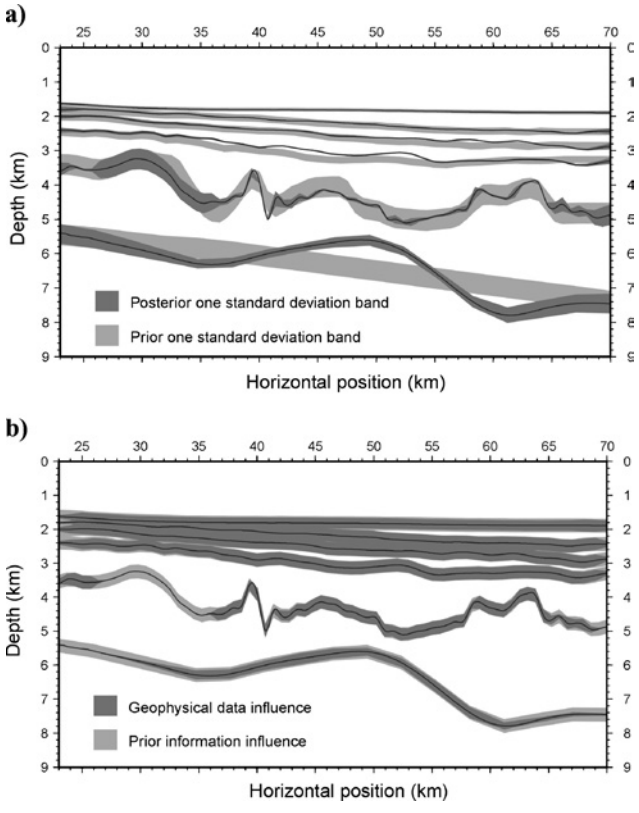

Figure 8. (a) Plot of the one standard deviation uncertainty band for interface depths associated with the prior and posterior models. (b) Plot of the impact of traveltime data and prior information on the estimated interface depths.

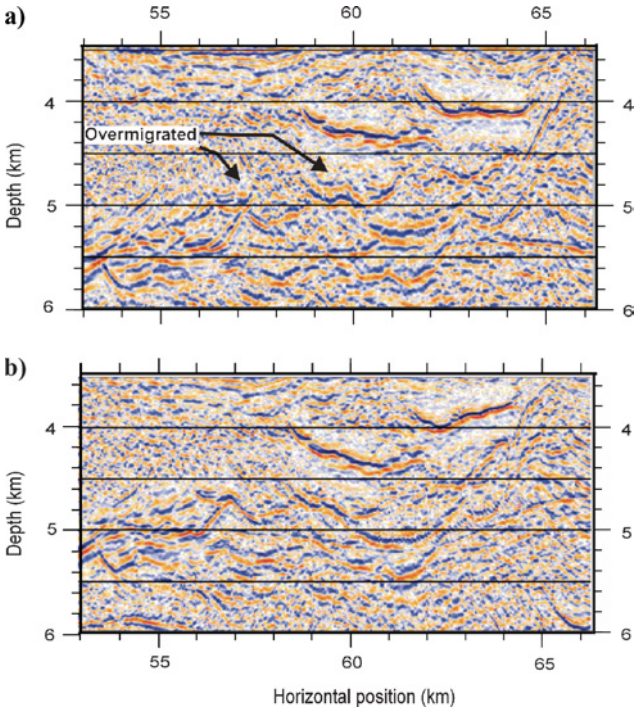

Figure 9. Comparison between the poststack depth-migrated section using (a) the velocity field derived from stacking velocities and (b) using the inverted tomographic velocity model. All other processing steps were identical for the two sections. Note over-migration of the sills shown in (a) and better reflector coherence in (b).

The basement structure in the model was estimated during the traveltime inversion, but it cannot be seen in the stacked profile, which is dominated by multiples below the system of sills. To model the basement, we used a first-arrival diving phase arriving at long offset (Figures 3 and 5) with particularly low amplitude, which is difficult to map into a zero-offset section using a conventional stacking or migration procedure.

DISCUSSION

It is useful to highlight differences between our approach of traveltime tomography and the common approach used in geostatistical inversion at reservoir level constrained by seismic wave-form data. In reservoirs, the objective is to simulate true scale heterogeneities of porosity and permeability; hence, covariance ranges should correspond to the actual medium characterization, and model regularization should not be considered. Also, in reservoir inversion the formulation may be done in either the time domain or the depth domain (if a good velocity model is already available). In the traveltime inversion shown here, covariance functions are defined accordingly, with a smoothing criterion. This approach can be used to

estimate the velocity field in areas without adequate ray coverage by interpolating between rays and by averaging velocities within Fresnel radius volumes, thereby improving the inversion results. Note that the goal of traveltime tomography is to estimate a smooth velocity model for migration or to provide a starting velocity model for wave-form inversion.

Another point to analyze is the limitations of the information provided by our likelihood term, equation 3, which is based on misfit evaluation of the traveltimes for several selected seismic phases. As integrals of the slowness along the raypaths, traveltimes in common seismic-acquisition geometries do not contain the short seismic-wavelength information on the medium (Jannane et al., 1989; Kosloff and Sudman, 2002). Also, the modeling component $\mathbf{g}(\mathbf{m})$ of the likelihood term is approximate, because ray-tracing traveltimes are an infinite-frequency approximation of wave traveltimes, so the slowness average in Fresnel volumes is not accounted for in the likelihood term. For this reason, it is useful to include the criterion on resolution capabilities of the technique into the prior statistical model, equation 2, by the nondiagonal terms of the covariance matrix.

There are limitations intrinsic to the optimization approach employed here, as well as limitations of the resolution and uncertainty analysis presented. If the posterior density is multimodal, convergence to a global maximum of the posterior density is not guaranteed. Also, the resolution and uncertainty analysis reflects the local statistics around a particular mode of the solution, rather than global statistics. However, the statistical inversion described here is more robust in this respect than conventional geophysical inversion that does not incorporate prior information. Prior information, which we model as a Gaussian density, constrains the model space, making the posterior density more regular. In addition to the quality of the prior information, a second aspect that contributes to regularity of the posterior density is the association of observed traveltime phases with particular ray phases in the model. This problem is more linear than the first-arrival traveltime problem, in which different ray phases are involved but not separated.

The validity of the Gaussian approximation of the posterior density used for the resolution and uncertainty analysis is related to the distance between the prior and optimal models. If we have a good prior model that significantly constrains the model space, and the optimal model obtained from the inversion is close to the prior model in such a way that deviations from a linear approximation of traveltimes are not strong, then the posterior density would be close to Gaussian. This is an advantage over conventional geophysical inversion since this method allows the combination of prior and geophysical information.

Monte Carlo methods for sampling the posterior density are not subjected to the limitations discussed above; therefore, they can be used for accurate computation of global posterior statistics and mode analysis. However, the computation times for Monte Carlo techniques are commonly much larger than those corresponding to optimization techniques, which can be a major difficulty for implementation of Monte Carlo approaches and their convergence to the posterior statistics. In particular, raypath and traveltime calculations in a heterogeneous medium require significant computation time, of the order of minutes on a workstation for the application shown in the preceding sections. Considering the number of model parameters involved, Monte Carlo sampling would require over 100 000 evaluations of the forward problem. Instead, our optimization approach requires only a few iterations of the forward problem solution to calculate the optimal model.

Finally, an interesting capability of the method presented here can be exploited if well logs are available along the line. In this case, the hard information of the well log can be incorporated into the prior model by reducing the model variance along the intersection of the model with the well. This guarantees that the result of the inversion will conform to the well logs as well as optimize the overall model to fit the traveltime data.

CONCLUSIONS

We present a methodology that combines geostatistical and geophysical information in the estimation of a seismic velocity-structural model. We describe spatially correlated velocities and interfaces statistically with a common multivariate Gaussian probability model, covariance functions, and prior expected values. Several types of information are incorporated into the prior statistical model: (1) the trend and variability of compressional velocities with depth in crossplots of logged well data from a nearby area, and (2) depths of major reflectors obtained from a preliminary processing of the seismic data. Covariance functions are defined to regularize the model according to decreasing tomographic resolution with depth of the layer. We also calculate posterior confidence intervals for the estimated interface depths and velocities and develop a measure for the relative impacts of the geophysical data and the prior information in the estimation.

Using this approach to traveltime tomography, we obtain an optimal two-dimensional velocity-structure model for a section along a seismic line in the northeast Atlantic margin area, improving the velocity estimates in comparison to the velocity model obtained from stacking velocities. The reflected seismic phases arriving at conventional offsets (up to 6 km) contributed information to the upper part of the model down to 4 km depth. Long-offset (up to 18 km) diving-wave phases constrained velocities for depths down to 8 km, including information on basement structure that cannot be identified in the stacked seismic image generated by conventional processing. Our optimal model explains the traveltime arrivals and, at the same time, honors the prior geostatistics provided for layer seismic velocities and layer interfaces.

ACKNOWLEDGMENTS

We acknowledge the BGS Rockall Consortium for providing the seismic data used in this study, in particular its coordinator, Ken Hitchen. We thank Conoco for providing crossplots from well log data used here to characterize the statistics of the compressional velocity. We used James Hobro's JIVE3D source codes for ray tracing, layer modeling, and most graphics, and coded the inversion and geostatistical parts of the method. This work has been conducted within the LITHOS Consortium research program (University of Cambridge–IPG Paris). We appreciate the comments by Paul Williamson and Richard Hobbs during our work. Thanks to Yonghe Sun, Aldo Vesnaver, Olivier Dubrule, Giuliana

Rossi, and an anonymous referee for their constructive reviews and corrections to the manuscript.

REFERENCES

Backus, G., and F. Gilbert, 1968, The resolving power of gross Earth data: Journal of the Royal Astronomical Society, **16**, 169–205.

Böhm, G., and A. Vesnaver, 1999, In quest of the grid: Geophysics, **64**, 1116–1125.

Böhm, G., P. Galuppo, and A. Vesnaver, 2000, 3D adaptive tomography using Delaunay triangles and Voronoi polygons: Geophysical Prospecting, **48**, 723–744.

Bosch, M., 1999, Lithologic tomography: From plural geophysical data to lithology estimation: Journal of Geophysical Research, **104**, 749–766.

———, 2004, The optimization approach to lithological tomography: Combining seismic data and petrophysical information for porosity prediction: Geophysics, **69**, 1272–1282.

Bosch, M., and J. McGaughey, 2001, Joint inversion of gravity and magnetic data under lithological constraints: The Leading Edge, **20**, 877–881.

Bosch, M., A. Guillen, and P. Ledru, 2001, Lithologic tomography: An application to geophysical data from the Cadomian belt of northern Brittany, France: Tectonophysics, **331**, 197–227.

Buland, A., and J. Omre, 2003, Bayesian wavelet estimation from seismic and well data: Geophysics, **68**, 2000–2009.

Chiles, J.-P., and P. Delfiner, 1999, Geostatistics: Modeling spatial uncertainty: John Wiley & Sons.

Constable, S. C., R. L. Parker, and C. G. Constable, 1987, Occam's inversion: A practical algorithm for generating smooth models from electromagnetic sounding data: Geophysics, **52**, 289–300.

Davis, M. W., 1987, Generating large stochastic simulations — The matrix polynomial approximation method: Mathematical Geology, **19**, 99–107.

Deutsch, C. V., and A. G. Journel, 1992, GSLIB, geostatistical software library and users' guide: Oxford University Press.

Dietrich, C. R., 1993, Computationally efficient generation of Gaussian conditional simulations over regular sample grids: Mathematical Geology, **25**, 439–451.

Docherty, P., 1992, Solving for the thickness and velocity of the weathering layer using 2-D refraction tomography: Geophysics, **57**, 1307–1318.

Dubrule, O., 2003, Geostatistics for seismic data integration in earth models: SEG Distinguished Instructor Short Course.

Farra, V., 1990, Amplitude computation in heterogeneous media by ray perturbation theory: A finite element approach: Geophysical Journal International, **103**, 341–354.

Hass, A., and O. Dubrule, 1994, Geostatistical inversion — A sequential method of stochastic reservoir modeling constrained by seismic data: First Break, **12**, 561–569.

Hobro, J., S. C. Singh, and T. A. Minshull, 2003, Three-dimensional inversion of combined reflection and refraction seismic traveltime data: Geophysical Journal International, **152**, 79–93.

Hubral, P., J. Schleicher, M. Tygel, and C. Hanitzsch, 1993, Determination of Fresnel zone from traveltime measurements: Geophysics, **58**, 703–712.

Hughes, S., P. J. Barton, and D. Harrison, 1998, Exploration in the Shetland-Faroe basin using densely spaced arrays of ocean-bottom seismometers: Geophysics, **63**, 490–501.

Isaaks, E., and R. Srivastava, 1989, An introduction to applied geostatistics: Oxford University Press.

Jannane, M., W. Beydoun, E. Crase, D. Cao, Z. Koren, E. Landa, M. Mendes et al., 1989, Wavelengths of earth structures that can be resolved from seismic reflection data: Geophysics, **54**, 906–910.

Kosloff, D., and V. Sudman, 2002, Uncertainty in determination of interval velocities from surface reflection seismic data: Geophysics, **67**, 952–963.

McCaughey, M., and S. Singh, 1997, Simultaneous velocity and interface tomography of normal-incidence and wide-aperture seismic traveltime data: Geophysical Journal International, **131**, 87–99.

Michelena, R. J., 1993, Singular value decomposition for cross-well tomography: Geophysics, **58**, 1655–1661.

Mosegaard, K., S. Singh, D. Snyder, and H. Wagner, 1997, Monte Carlo analysis of seismic reflections from Moho and the W reflector: Journal of Geophysical Research, **102**, 2969–2981.

Press, W. H., S. A. Teukolsky, W. T. Vetterling, and B. P. Flannery, 1997, Numerical recipes in Fortran: Cambridge University Press.

Rossi, G., P. Corubolo, G. Böhm, E. Ceragiolli, P. Dell'Aversana, S. Morandi, F. Polleto, and A. Vesnaver, 2001, Joint 3D inversion of SWD and surface seismic data: First Break, **19**, 453–459.

Scales, J., and R. Snieder, 1997, To Bayes or not to Bayes?: Geophysics, **62**, 1045–1046.

Scales, J., and L. Tenorio, 2001, Prior information and uncertainty in inverse problems: Geophysics, **66**, 389–397.

Spetzler, J., and R. Snieder, 2004, The Fresnel volume and transmitted waves: Geophysics, **69**, 643–663.

Stork, C., 1992, Singular value decomposition of the velocity-reflector depth trade-off, Part 2: High-resolution analysis of a generic model: Geophysics, **57**, 933–943.

Tarantola, A., 1987, Inverse problem theory: Methods for data fitting and model parameter estimation: Elsevier.

Torres-Verdin, C., M. Victoria, G. Merletti, and J. Prendel, 1999, Trace-based and geostatistical inversion of 3D seismic data for thin sand delineation: An application in San Jorge basin, Argentina: The Leading Edge, **18**, 1070–1077.

Trinks, I., S. Singh, C. Chapman, P. Barton, M. Bosch, and A. Cherrett, 2004, Adaptive traveltime and ray-parameter inversion of densely sampled 2-D seismic data: 66th Conference and Exhibition, European Association of Geophysicists and Engineers.

Vasco, D. W., J. E. Peterson Jr., and E. L. Majer, 1996, Non-uniqueness in traveltime tomography: Ensemble inference and cluster analysis: Geophysics, **61**, 1209–1227.

Zang, J., and M. N. Toksöz, 1998, Nonlinear refraction traveltime tomography: Geophysics, **63**, 1726–1737.

Zelt, C., and P. Barton, 1998, Three-dimensional seismic refraction tomography: A comparison of two methods applied to data from the Faroe Basin: Journal of Geophysical Research, **99**, 9263–9278.

Zou, H., 2003, Multiscale tomography: Geophysics, **68**, 1639–1649.